JOURNAL OF APPLIED POLYMER SCIENCE VOL. 17, PP. 3157–3174 (1973)

An Analysis for the Calendering of Non-Newtonian Fluids

WILLIAM W. ALSTON, JR.,* and KENNETH N. ASTILL,
Department of Mechanical Engineering, Tufts University, Medford, Massachusetts 02155

Synopsis

Equations are derived to predict the one-dimensional behavior of a hyperbolic tangent fluid model flowing between calendering rollers. The equations were solved numerically on a computer, and results were obtained for maximum roller pressure and the exit thickness of the fluid sheet as a function of roller speed and reservoir size for three polymers. The numerical integration employed Gauss-Legendre quadrature and a cascading iteration scheme to solve equations in which unknowns appeared in the limits of the integrals. Unlike existing power law solutions, these results show a definite relation between roller speed and exit thickness.

INTRODUCTION

In the past thirty years, there have been numerous attempts to analyze fluid flow between rotating cylinders, or "calendering." Calendering is a steady-state process, common to the plastics industry, by which softened material is squeezed into thin sheets by one or more pairs of driven rollers[1] (see Fig. 1). The analyses of these related problems have dealt with viscous Newtonian[2] and non-Newtonian fluids[2] having flow properties approximated by various constitutive models.

Chong[3] reviewed previous work and considered calendering of non-Newtonian power law fluids. He indicated that the use of a power law model is limited and the accuracy of solutions based on this model may suffer as a result. More sophisticated models exist but, because they are complex, a more tractable substitute for the power law is still needed.

The goal of this work was to discover a better non-Newtonian fluid model, derive the equations relating to the behavior of that fluid between calendering rollers, and to solve these equations for exit thickness and roller forces.

Put in very specific terms, the present objective is to find the sheet thickness at the exit from the rollers (h_1) and the maximum fluid pressures as a function of reservoir height (H), minimum roller separation (H_0), roller surface speed (U), and fluid properties. These symbols are identified in the illustration of the system model, Figure 2.

* Present address: Polaroid Corporation, Cambridge, Massachusetts.

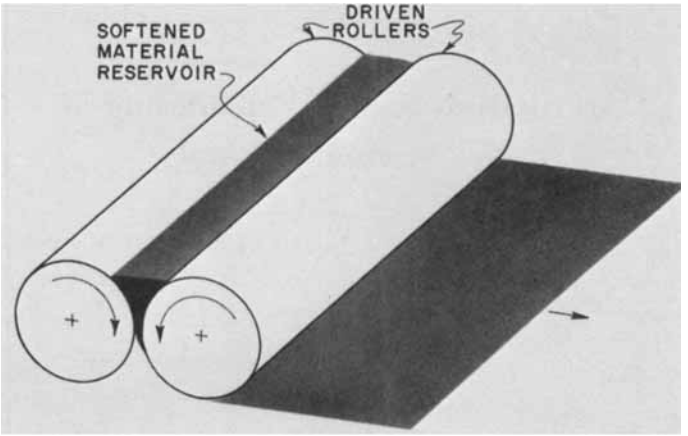

Fig. 1. The calendering process.

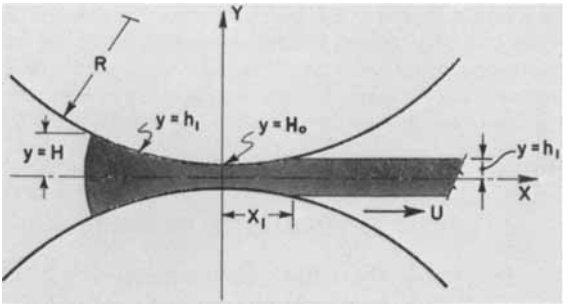

Fig. 2. Symmetrical calendering rollers showing symbols used in analysis.

THE HYPERBOLIC TANGENT MODEL

The fluid in question is assumed to be a pseudoplastic and to have the following characteristics: (1) It is non-Newtonian. The shear stress, τ, can be expressed for the one-dimensional case as

$$\tau = \eta \left(\frac{\partial v_x}{\partial y} \right) = \eta \dot{\gamma} \tag{1}$$

where η is the apparent viscosity and $\dot{\gamma}$ is the shear rate; (2) η decreases with increasing $\dot{\gamma}$; (3) first and second Newtonian viscosities are evident. (In Newtonian fluids η is constant. For the polymers considered, η approaches a constant for small $\dot{\gamma}$, and a second, smaller constant for large $\dot{\gamma}$. The viscosity in these flat regions will be referred to as the first and second Newtonian viscosities, respectively.)

It is possible to measure η for non-Newtonian fluids as a function of $\dot{\gamma}$. This was done (using Rotovisko and Burrell viscometers) for several polymers of interest to the problem. Graphs of these data are shown in Figure 3.

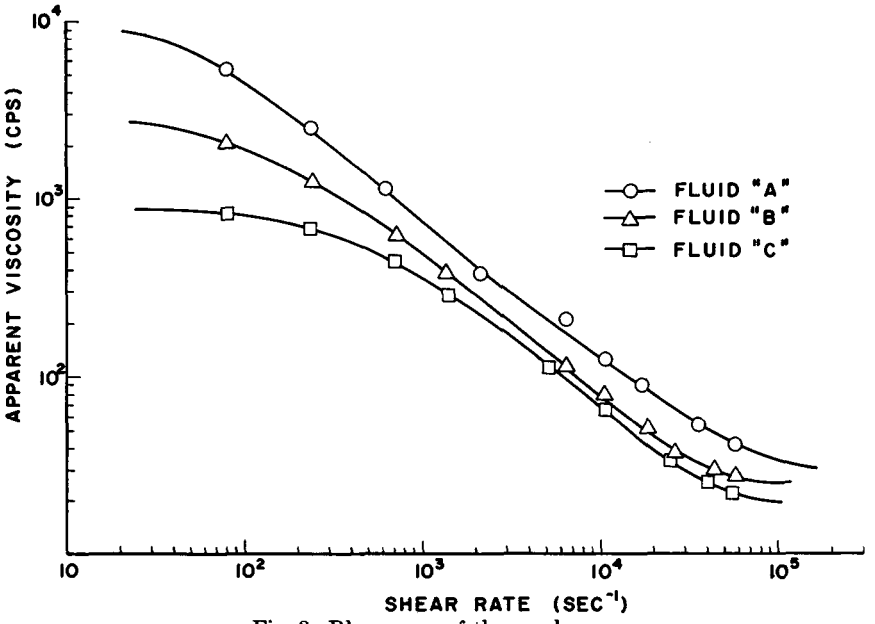

Fig. 3. Rheograms of three polymers.

The power law model,

$$\eta = k|\dot{\gamma}|^{n-1} \tag{2}$$

where n and k are constants, fails to show curve fluctuations typical of some families of pseudoplastics. A single power law approximation would appear as a straight line on the log–log coordinates of Figure 3.

However, these viscometer data can be fit conveniently by a curve having the form

$$\eta = A - B \tanh\left(\frac{\dot{\gamma}}{k}\right)^n \tag{3}$$

which will be referred to as the tanh model. The tanh model reduces to the first and second Newtonian viscosities at very low and very high shear rates, respectively, and offers a close approximation to the apparent viscosities during the several intermediate decades.

In order to fit viscometer data by this model, four constants must be found: A, B, n, and k. The constant A is simply the first Newtonian viscosity. Constant B is the difference between the first and second Newtonian viscosities. Note that the first and second Newtonian viscosities can be read graphically and constitute the values of η at the leveling-off points. Constants n and k were found by program MODFIT.

Program MODFIT is an iteration scheme based on a criterion of least error:

$$\sum_{i=1}^{N} \left| \frac{\eta_{\text{data}} - \eta_{\text{calc}}}{\eta_{\text{data}}} \right| \rightarrow \text{minimum.} \tag{4}$$

Computations were made for the three fluids under consideration. The computed* constants for the three fluids, designated A, B and C were

	n	k	A	B
fluid A	0.25	3.90	8000	7965
fluid B	0.29	6.70	2700	2678
fluid C	0.35	15.10	850	838

All computations were made on a Control Data 3600 computer using time sharing.

DERIVATION

A hydrodynamic analysis of calendering will now be developed beginning with the Gaskel[1,2] method for general non-Newtonian flow and concluding with the equations for maximum pressure and film thickness using the tanh model. The value of knowing the maximum pressure can be illustrated by observing the typical experimental pressure profile shown in Figure 4.[1] Given the maximum pressure and inlet and exit points on the rollers, this curve can be estimated and integrated to give roller forces.

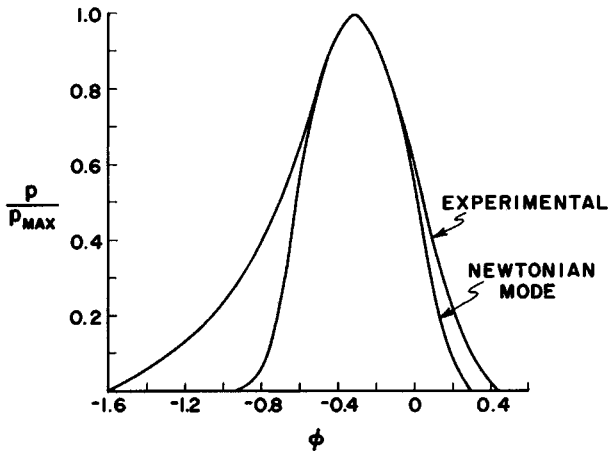

Fig. 4. Typical pressure profile for fluid between calendering rollers (see ref. 1).

Considering the flow to be two-dimensional, the equation for the x-component of momentum in the absence of body forces can be written as

$$\rho\left(\frac{\partial V_x}{\partial t} + V_x\frac{\partial V_x}{\partial x} + V_y\frac{\partial V_x}{\partial y}\right) = \frac{-\partial P}{\partial x} + \left(\frac{\partial \tau_{xx}}{\partial x} + \frac{\partial \tau_{yx}}{\partial y}\right). \quad (5)$$

The continuity equation is

$$\frac{\partial \rho}{\partial t} + \frac{\partial}{\partial x}(\rho V_x) + \frac{\partial}{\partial y}(\rho V_y) = 0. \quad (6)$$

We now introduce five simplifying assumptions:

(A) Flow is incompressible and steady. Continuity reduces to

$$\frac{\partial V_x}{\partial x} + \frac{\partial V_y}{\partial y} = 0 \tag{7}$$

and the x-component of momentum equation reduces to

$$\rho\left(V_x \frac{\partial V_x}{\partial x} + V_y\left(\frac{\partial V_x}{\partial y}\right)\right) = \frac{-\partial P}{\partial x} + \left(\frac{\partial \tau_{xx}}{\partial x} + \frac{\partial \tau_{yx}}{\partial y}\right). \tag{8}$$

(B) Non-Newtonian viscosity is considered to be a function of the rate of shear. This function is the tanh model.

(C) The acceleration terms of the momentum equation are neglected because viscous forces are large compared to inertia forces.

(D) Since V_x varies much more in the y-direction than in the x-direction, second derivatives of V_x with respect to x can be shown to be small compared to second derivatives of V_x with respect to y.

(E) Pressure is constant in the y-direction. Therefore, $\partial P/\partial x$ is also constant in the y-direction.

From the above assumptions, the equation for the x-component of momentum for a non-Newtonian fluid becomes

$$\frac{\partial P}{\partial x} = \frac{\partial \tau_{yx}}{\partial y} = \frac{\partial}{\partial y}\left(\eta \frac{\partial V_x}{\partial y}\right) \tag{9}$$

where η is the non-Newtonian viscosity defined in eq. (1). Note that hereafter the subscripts on τ will be dropped.

Integrating eq. (9) with respect to y for constant x, and utilizing assumption E,

$$y\left(\frac{\partial P}{\partial x}\right) = \tau = \eta\left(\frac{\partial V_x}{\partial y}\right) + C. \tag{10}$$

Since the flow is symmetrical about the x-axis,

$$\left(\frac{\partial V_x}{\partial y}\right)_{y=0} = 0.$$

Hence $\tau(0) = 0$ and $C = 0$.

Next we eliminate the variable y in eq. (10). From eq. (9),

$$\frac{\partial P}{\partial x} = \frac{\partial \tau}{\partial y}$$

$$\frac{\partial V_x}{\partial y} = \frac{\partial V_x}{\partial \tau}\frac{\partial \tau}{\partial y}$$

or

$$\frac{\partial V_x}{\partial y} = \frac{\partial V_x}{\partial \tau}\left(\frac{\partial P}{\partial x}\right)$$

With eq. (10), this becomes

$$\frac{\partial V_x}{\partial \tau} = \frac{1}{\left(\frac{\partial P}{\partial x}\right)} \frac{\tau}{\eta}. \tag{11}$$

Integrating (11) across the gap from τ_w to τ and U to V_x, and noting that $\partial P/\partial x$ is constant through this interval, an expression for V_x is obtained:

$$V_x = U - \frac{1}{\left(\frac{\partial P}{\partial x}\right)} \int_{\tau}^{\tau_w} \left(\frac{\tau}{\eta}\right) d\tau \tag{12}$$

where U is the roller surface speed.

The volume rate of flow at a given location, x, can be expressed as

$$Q = 2 \int_0^h V_n dy. \tag{13}$$

It is convenient to integrate eq. (13) over τ. Introducing the derivative of eq. (10) and adjusting the limit transforms eq. (13) to

$$Q = \frac{2}{\left(\frac{\partial P}{\partial x}\right)} \int_0^{\tau_w} V_x d\tau. \tag{14}$$

Now, using eq. (12) for V_x in eq. (14), the flow rate becomes

$$Q = \frac{2U}{\left(\frac{\partial P}{\partial x}\right)} \tau_w - \frac{2}{\left(\frac{\partial P}{\partial x}\right)^2} \int_0^{\tau_w} \int_{\tau}^{\tau_w} \frac{\tau}{\eta} d\tau d\tau; \tag{15}$$

and from eq. (10), with $y = h$ at $\tau = \tau_w$,

$$\tau_w = \left(\frac{\partial P}{\partial x}\right) h. \tag{16}$$

For convenience, we introduce the following dimensionless form of x:

$$\phi = \frac{x}{\sqrt{2RH_0}}. \tag{17}$$

Using the minimum gap H_0 and the first term of the binomial expansion for the roller curvature,

$$h = H_0 + \frac{x^2}{2R}. \tag{18}$$

Combining eqs. (17) and (18),

$$h = H_0(1 + \phi^2) \tag{19}$$

or

$$\phi^2 = \frac{h}{H_0} - 1. \tag{20}$$

Substituting (19) for h in (16),

$$\tau_w = H_0(1 + \phi^2)\left(\frac{\partial P}{\partial x}\right). \tag{21}$$

Then, rewriting eq. (15) with (21),

$$Q = 2UH_0(1 + \phi^2) - \frac{2}{\left(\frac{\partial P}{\partial x}\right)^2}\int_0^{\tau_w}\int_\tau^{\tau_w}\left(\frac{\tau}{\eta}\right)d\tau d\tau. \tag{22}$$

At the point where the fluid leaves the roll surface, x_1, the sheet thickness has been established as h_1. At this point, τ_w must necessarily go to 0, causing $\partial P/\partial x$ to become zero across the gap, eq. (21). Consequently, τ must be zero for all y to satisfy eq. (10), and we deduce that the velocity is uniform across the gap and necessarily equal to the wall speed $U \cos \theta_1 \approx U$. The volume flow can be expressed as

$$Q = 2Uh_1 \tag{23}$$

or

$$h_1 = \frac{Q}{2U}. \tag{24}$$

If we identify the value of ϕ at x_1 as ϕ_1, then

$$\phi_1 = \frac{x_1}{\sqrt{2RH_0}} \tag{25}$$

or, in the form of eq. (20),

$$\phi_1^2 = \frac{h_1}{H_0} - 1. \tag{26}$$

Introducing eq. (24) into eq. (26),

$$\phi_1^2 = \frac{Q}{2UH_0} - 1. \tag{27}$$

If eq. (27) is inserted into eq. (22) at $\phi = \phi_1$, it is evident that the integral term on the right-hand side is zero at $x = x_1$. This is significant. While it is evident that at x_1, $\tau = \tau_w$ and the integral disappears, it must be noted that at x_1, $\partial P/\partial x$ is also zero.

Using eq. (27) to express Q, eq. (28) can be written as

$$Q = 2UH_0(1 + \phi_1^2). \tag{28}$$

Combining eq. (28) with (22) to eliminate Q,

$$\phi^2 - \phi_1{}^2 = \frac{1}{UH_0}\left(\frac{\partial P}{\partial x}\right)^2 \int_0^{\tau_w}\int_\tau^{\tau_w}\left(\frac{\tau}{\eta}\right) d\tau d\tau \tag{29}$$

or

$$\phi^2 - \phi_1{}^2 = \frac{1}{UH_0}\left(\frac{\partial P}{\partial x}\right)^2 \int_0^{\tau_w}\frac{\tau^2}{\eta}\, d\tau. \tag{30}$$

Equation (30) comes from eq. (29) by the following relation (see, for example, reference,[1] pp. 234–235):

$$\int_0^{\tau_w}\int_\tau^{\tau_w} f(\tau)d\tau d\tau = \int_0^{\tau_w}\tau f(\tau)d\tau.$$

Proof: $$I = \int_0^{\tau_w}\int_\tau^{\tau_w} f(\tau)d\tau d\tau = \int_0^{\tau_w}\left[\int_0^{\tau_w} f(\tau)d\tau - \int_0^{\tau} f(\tau)d\tau\right] d\tau$$

$$= \int_0^{\tau_w}\left[\int_0^{\tau_w} f(\tau)d\tau\right] d\tau = \int_0^{\tau_w}\int_0^{\tau} f(\tau)d\tau d\tau$$

$$= \tau_w\int_0^{\tau_w} f(\tau)d\tau - \int_0^{\tau_w}\int_0^{\tau} f(\tau)d\tau d\tau.$$

It is possible to transform the double integral into a single integral by using the convolution theorem:[4]

Let

$$g(\tau_w) = \int_0^{\tau_w}(\tau_w - \tau)f(\tau)d\tau;$$

then

$$\mathfrak{L}_g(\tau_w) = \frac{1}{S^2}f(\tau) = \frac{F(S)}{S^2}$$

$$\mathfrak{L}^{-1}\frac{F(S)}{S^2} = g(\tau_w) = \int_0^{\tau_w}\int_0^{\tau} f(\tau)d\tau d\tau.$$

With this, the expression I is

$$I = \tau_w\int_0^{\tau_w} f(\tau)d\tau - \int_0^{\tau_w}(\tau_w - \tau)f(\tau)d\tau$$

$$I = \int_0^{\tau}\tau f(\tau)d\tau.$$

The tanh fluid model, stated in eq. (3), can now be entered in eq. (30):

$$\phi^2 - \phi_1{}^2 = \frac{1}{UH_0}\left(\frac{\partial P}{\partial x}\right)^2 \int_0^{\tau_w}\frac{\tau^2}{A - B\tanh\dfrac{\dot\gamma^n}{k}}\, d\tau \tag{31}$$

or

$$\frac{\partial P}{\partial x} = \left[\frac{1}{UH_0(\phi^2 - \phi_1^2)} \int_0^{\tau_w} \frac{\tau^2}{A - B \tanh \frac{\dot{\gamma}^n}{k}} d\tau \right]^{1/2}. \tag{32}$$

Using the expression in eq. (21) for τ_w,

$$\frac{\partial P}{\partial x} = \left[\frac{1}{UH_0(\phi^2 - \phi_1^2)} \int_0^{H_0(1+\phi^2)\frac{\partial P}{\partial x}} \frac{\tau^2}{A - B \tanh \frac{\dot{\gamma}^n}{k}} d\tau \right]^{1/2}. \tag{33}$$

Using eq. (17), we can write

$$\frac{dP}{d\phi} = (\sqrt{2RH_0}) \frac{\partial P}{\partial x}. \tag{34}$$

Consequently,

$$\frac{dP}{d\phi} = \sqrt{2RH_0} \left[\frac{1}{UH_0(\phi^2 - \phi_1^2)} \int_0^{H_0(1+\phi^2)\left(\frac{\partial P}{\partial x}\right)} \frac{\tau^2}{A - B \tanh \frac{\dot{\gamma}^n}{k}} d\tau \right]^{1/2}. \tag{35}$$

From the above equations, we cannot expect to obtain a closed form solution for maximum pressure and ϕ_1. However, given that the pressure is zero at the edge of the reservoir ($\phi = \phi_H$) and at the exit from the rollers ($\phi = \phi_1$), and, as previously stated, the pressure reaches a maximum at ϕ_1, then

$$\int_{\phi 1}^{0} \left(\frac{dP}{d\phi}\right) d\phi + \int_0^{-\phi_1} \left(\frac{dP}{d\phi}\right) d\phi + \int_{-\phi_1}^{-\phi_H} \left(\frac{dP}{d\phi}\right) d\phi = 0$$

or

$$2 \int_{\phi_1}^{0} \left(\frac{dP}{d\phi}\right) d\phi + \int_{-\phi_1}^{-\phi_H} \left(\frac{dP}{d\phi}\right) d\phi = 0. \tag{36}$$

Equation (36) makes possible the numerical solution presented in the next section.

SOLUTION

The numerical solution is accomplished by choosing the limit ϕ_1 of eq. (36), making an initial guess for ϕ_H, and iterating ϕ_H by modified false position until eq. (36) converges to zero. This would be a reasonably straightforward process except for three major problems. First, as shown in eq. (33), $\delta P/\delta x$ equals a function containing an integral with the same $\delta P/\delta x$ in the upper limit. It is not separable. Second, this integral within an integral must be solved for each iteration step. Finally, $\dot{\gamma}$ is a function of τ and must be solved for in each step of the integration in eq. (33).

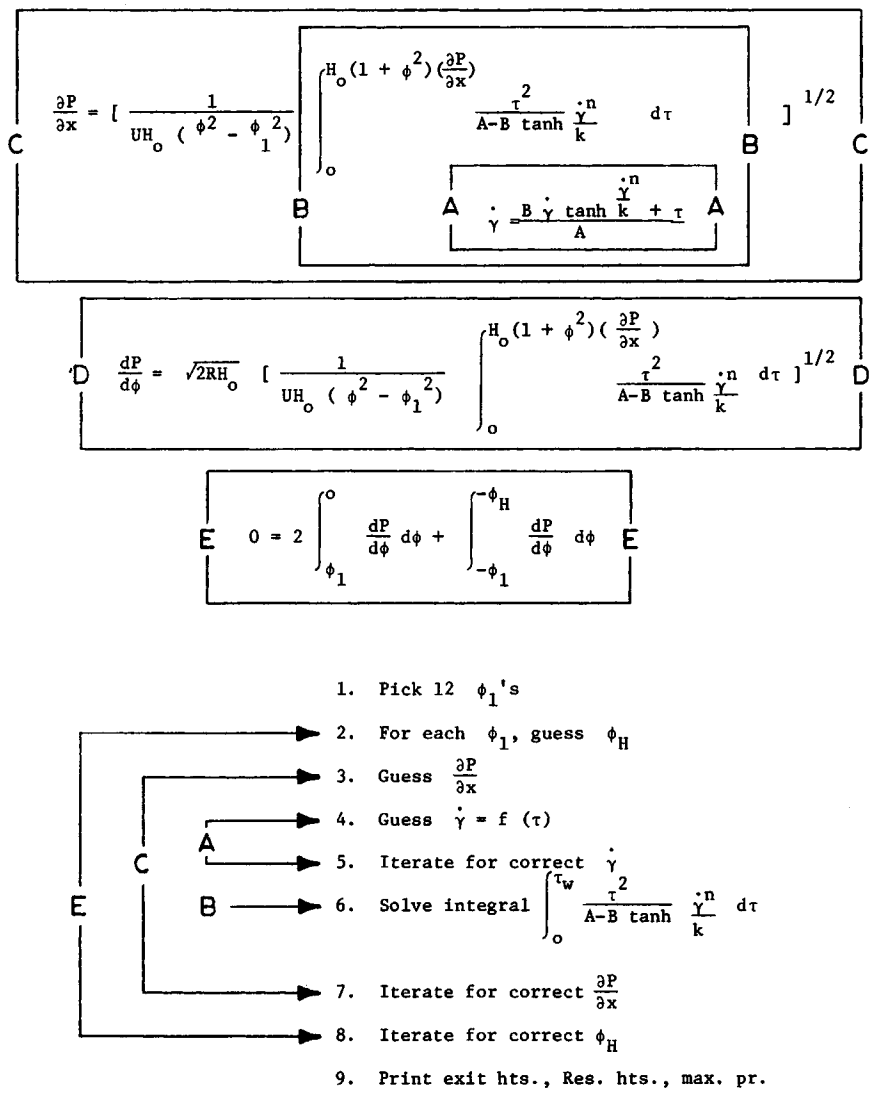

Fig. 5. Iteration loops used for the computer solution.

The problem is depicted schematically in Figure 5. Box E shows the conditions of the ultimate solution, the correct limit ϕ_H for each selected ϕ_1. The ϕ_1's were equispaced in a range of interest, as determined by a previous power law solution, corresponding to values of h_1/H_0 between 1.0 and 1.24. It is important in terms of computer time to make a close guess of ϕ_H for each ϕ_1, and this was accomplished by fitting a third-order least-squares polynomial to h_1/H_0 versus h/H_0 obtained from the analysis of a power law model by Branzinski et al.[5]

Integration in box E is done with a single application of four-point Gauss-Legendre quadrature in the main drive program called QUAD. With ϕ_1

and ϕ_H determined, the four values of ϕ at which $dP/d\phi$ must be evaluated are known and correspond to the roots of the Legendre polynomial of degree four.[6]

At each of these four values, the integral in box B must be solved by calling subroutine SIMPSON. Again, Gauss-Legendre quadrature is used. A guess of $\partial P/\partial x$ is made in order to get an initial value for the upper limit. With the range of integration known in terms of τ, the four roots of the Legendre polynomial yield the four values of τ at which the integrand is to be evaluated in the quadrature.

For each τ, a value of $\dot{\gamma}$ is guessed and set in the right-hand side of eq. (3). as given in box A. This is solved for the new $\dot{\gamma}$ on the left. The iteration proceeds by putting the new value of $\dot{\gamma}$ on the right and repeating the process until the left and right sides differ by less than 1%. This process of successive approximations is carried out in subroutine SUCCA.

Note that guesses are made in boxes E through A and now begin to converge in cascading subroutines from inside out, from boxes A through E. One should pay particular attention to this subroutine structure as depicted in the bottom of Figure 5.

With the four integrands available, the quadrature integration in subroutine SIMPSON can now be carried to completion. With box B evaluated, the right-hand portion of the expression in box C can be calculated, and the value of $\partial P/\partial x$ compared to the assumed value. Subroutine DPDX carries this successive approximation iteration forward until the error between the left and right sides of the expression in box C is less than 1%. A curve pivoting procedure is incorporated into the iteration to accelerate convergence.

With the proper $\partial P/\partial x$ for each ϕ and the expression in C determined, it is a simple matter to obtain $dP/d\phi$ with eq. (35) (box D).

Control is now returned to QUAD for the last step in the calculation loop, the iteration of the expression in box E, eq. (36). As previously stated, QUAD employs a four-point Gauss-Legendre quadrature. Iteration of ϕ_H is also carried out in this program, and each time a new ϕ_H is tried, the entire loop is repeated until the expression in box E is zero using a 3% error criterion. (That is, the entire subroutine cascade hierarchy is employed: QUAD to DPDX to SIMPSON to SUCCA and back again in reverse order.) As the value of ϕ_H is known approximately, this is not as difficult as it might in initially appear. Furthermore, once ϕ_1 is chosen, it is not necessary to recompute the first integral in box E as it does not involve ϕ_H.

A comment should be made here regarding a possible singularity in the expression in box C for $\partial P/\partial x$. When $\phi = \pm\phi_1$, the denominator on the right goes to zero. It was noted in the discussion following eq. (27) that $\partial P/\partial x \to 0$ as $\phi \to \pm\phi_1$. That is, the integral in box C goes to zero faster than the denominator $\phi^2 - \phi_1^2$ as $\phi \to \pm\phi_1$. This also indicates that there is a pressure maximum or minimum at $\pm\phi_1$. Based on physical reasoning and results for Newtonian flow, we assume that the curve reaches a maximum at $\phi = -\phi_1$ and goes to the minimum (zero pressure) at $\phi = +\phi_1$.

We have established a value of ϕ_H for each ϕ_1. We can calculate the gap width at $\pm\phi_1$ which will be the thickness of the film at exit. Assuming this to be the final film thickness, h_1 can be found from eq. (26),

$$h_1 = H_0(\phi_1^2 + 1)$$

and with eq. (25),

$$x_1 = \phi_1\sqrt{2RH_0}.$$

Reservoir height H can be found using ϕ_H in the same way:

$$H = H_0(\phi_H^2 + 1)$$

and

$$x_H = \phi_H\sqrt{2RH_0}.$$

Maximum pressure can be found as the value of either integral in eq. (36) (box E). That is,

$$P_{\max} = \int_{-\phi_1}^{\phi_H} dP = 2\int_0^{\phi_1} dP.$$

As these integrals were evaluated in the calculation process, it is a simple matter to print out the result for each ϕ_1.

Listing of programs and subroutines QUAD, DPDX, SIMPSON, and SUCCA are not presented in the paper but are available in reference 7.

RESULTS

From the programs outlined in the last section, output was produced using constants for the hyperbolic tangent model for the three polymers of Figure 3. The geometry used is shown in Figure 2, where $H_0 = 0.0016$ in., R = apparent roller, radius = 0.5 in., and U varies from 5.0 in./sec to 50.0 in./sec. This output, involving three or more roller speeds for each polymer, has been presented in the graphs of Figures 6 through 11.

For each polymer, there are curves giving the dimensionless ratio of the exit height h_1 to the gap between rollers, H_0, as a function of the reservoir height ratio H/H_0 for a family of roller surface speeds, U (Figs. 6, 7, and 8). A second set of curves shows the relation between the maximum pressure, lb-ft/in.^{2} versus the reservoir height ratio for the three polymers at several speeds (Figs. 9, 10, and 11).

On examining the solutions for exit heights graphed in Figures 6, 7, and 8, it is evident that when the ratio of reservoir height to gap (H/H_0) exceeds 20, the effect of increasing the reservoir height on the exit thickness is small. This suggests that the maximum practical thickness of a calendered sheet is controlled more by roller gap than by reservoir height.

These solutions are very close to those calculated in previous work involving power law fluids,[5] with this exception: these new calculations show significant changes in the H-versus-h_1 curves as the roller surface speed is

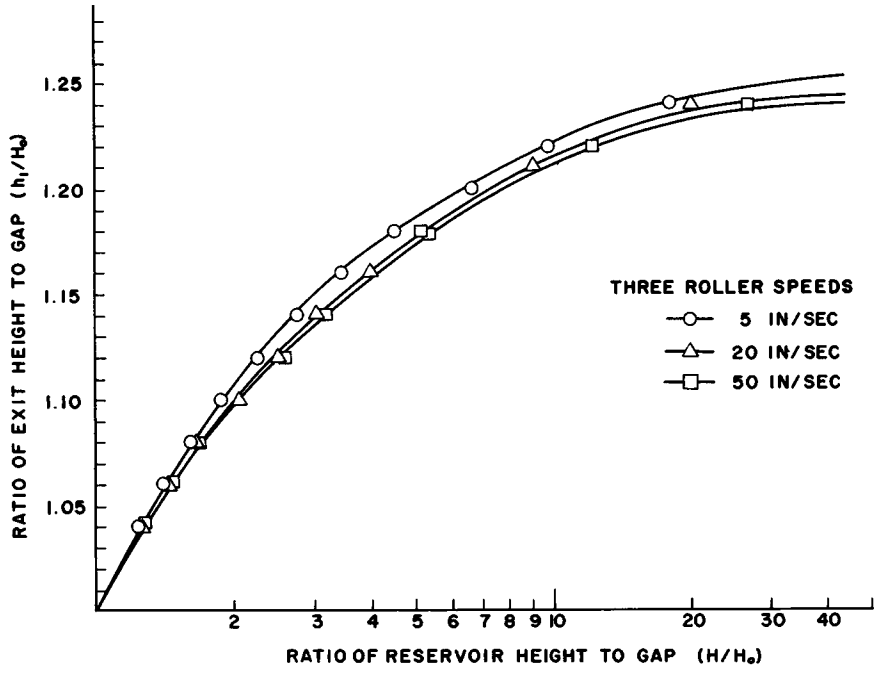

Fig. 6. Exit height of sheet for fluid A.

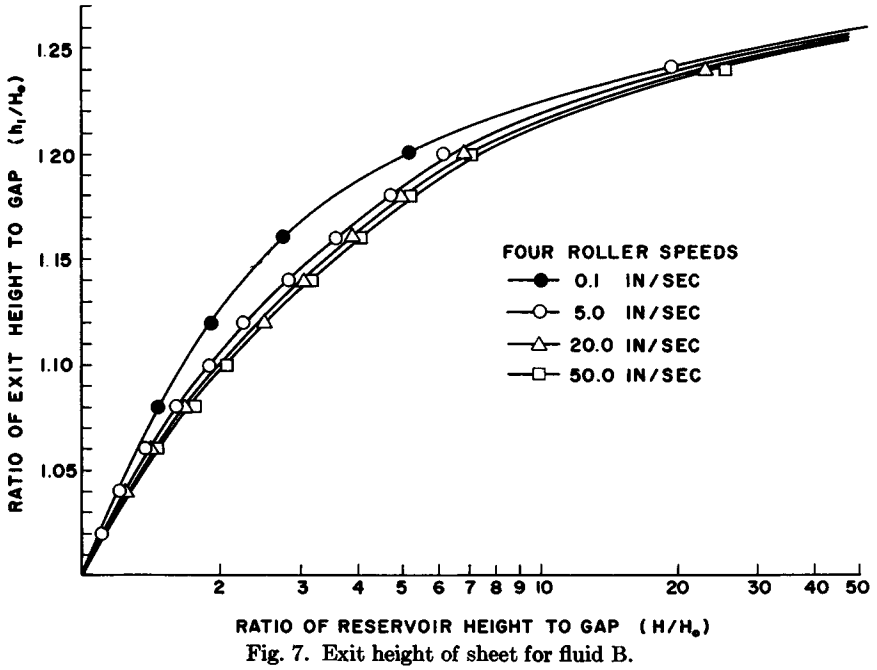

Fig. 7. Exit height of sheet for fluid B.

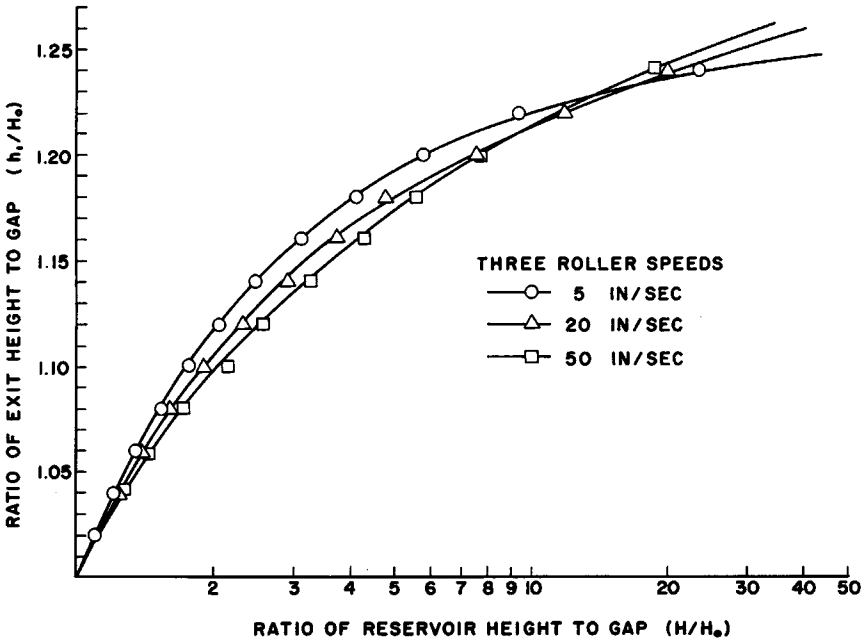

Fig. 8. Exit height of sheet for fluid C.

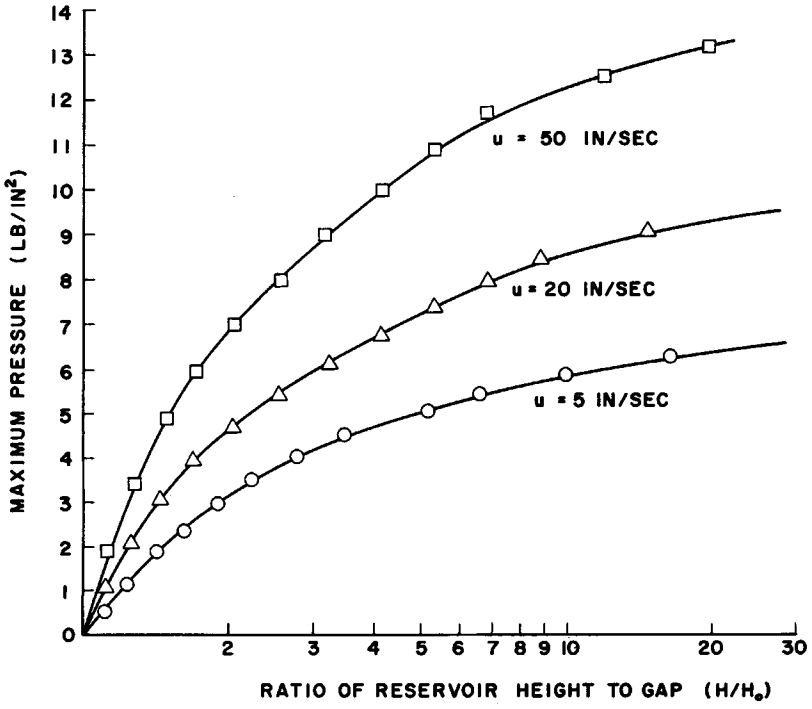

Fig. 9. Maximum calendering pressure for fluid A.

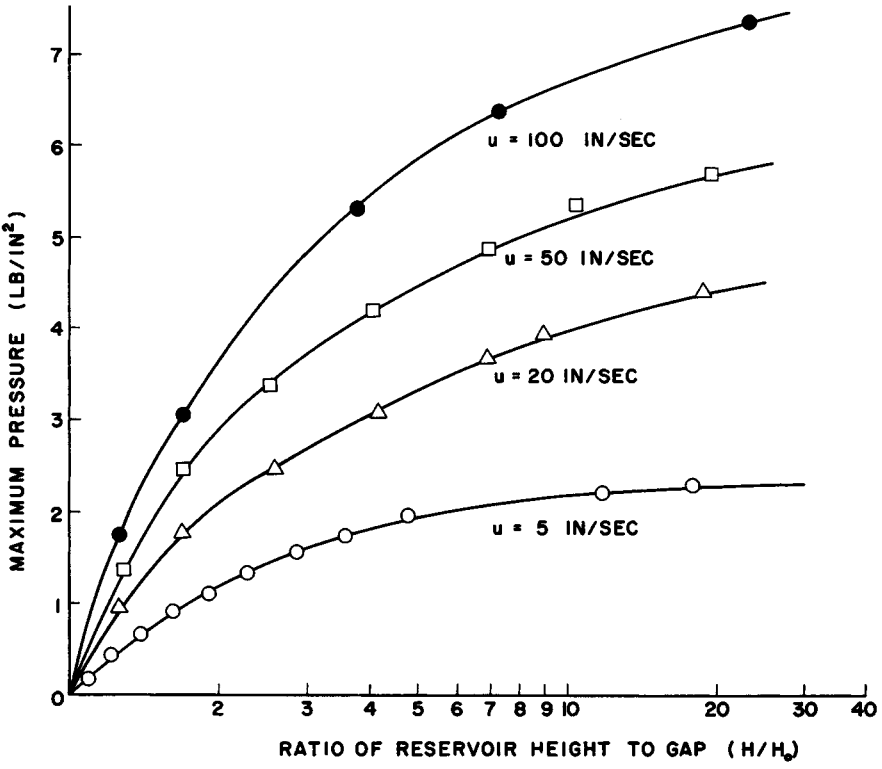

Fig. 10. Maximum calendering pressure for fluid B.

changed. Power law solutions show no such changes. They depend only on power law slope for a given geometry.

Maximum pressures, graphed in Figures 9, 10, and 11, were strongly affected by speed and viscosity. As the roller surface speeds increased from 5 in./sec to 50 in./sec, the maximum pressures increased two to three times for the fluids considered. Maximum pressures for fluid A were nearly double those at the same conditions for the less viscous fluid C.

A NOTE ON THE NUMERICAL SOLUTION

When you consider the problem which has been solved here, your first reaction is that you will require an explicit shear stress distribution or velocity profile. Using the four-point quadrature the problem was one of finding shear rates at a few discrete values of the shear stress. These values of shear stress are known as soon as the local pressure gradient is assumed. Then the problem is to cause the pressure gradient created by the shear stresses to match the pressure gradient which established them. Consequently, it is not necessary to generate a functional shear stress distribution across the gap.

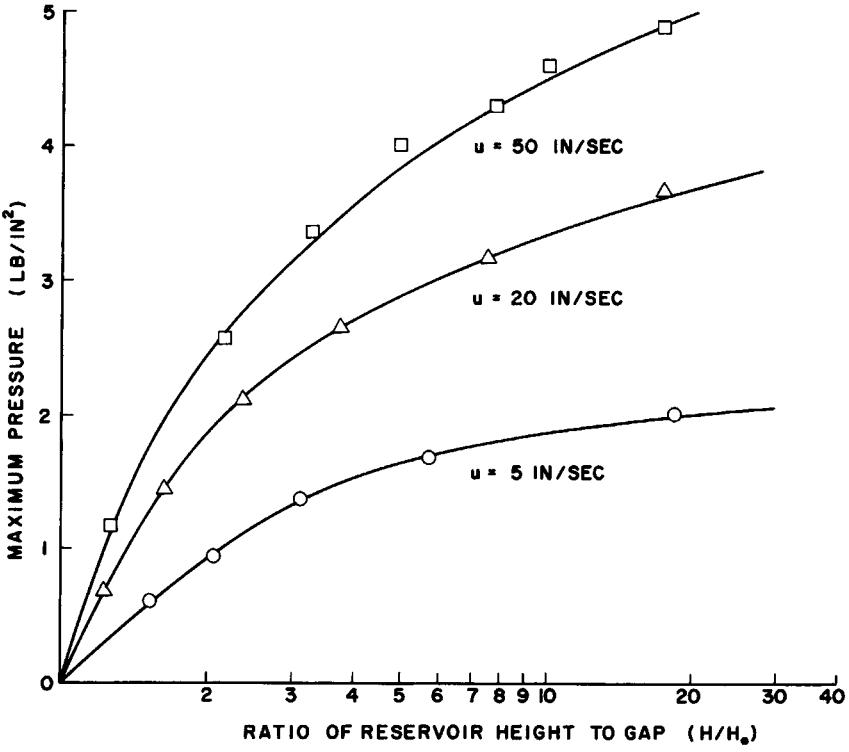

Fig. 11. Maximum calendering pressure for fluid C.

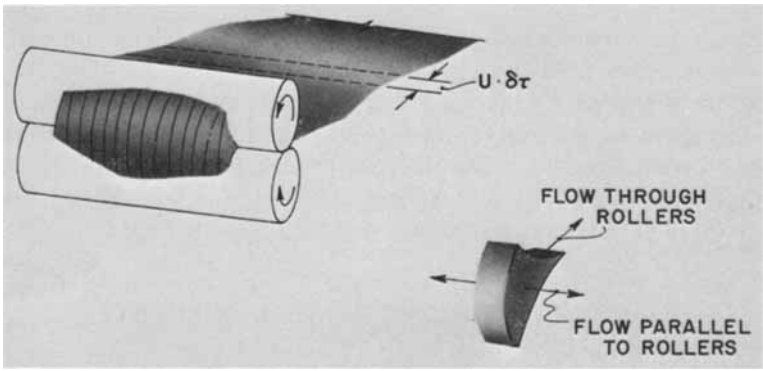

Fig. 12. Two-dimensional model for calendering.

A second point is the temptation to integrate pressure along the x-direction by open integration formulae, "shooting" pressure curves until at $\phi = \phi_1$, $P = 0$. While this suggests the advantage that a pressure distribution would be found along the calendering surface, it presents certain problems. Not only would it require the iteration to validate guesses of ϕ_H but it would require repeated iteration of the pressure at ϕ_1. The present method

employs closed form integration forcing pressure to match the boundary conditions.

FUTURE EXTENSION OF WORK

The primary follow-up of this analysis should be an experimental evaluation of the results. The instrumentation for such a project was considered beyond the scope of the work.

The solutions presented here should be useful not only in predicting calendered sheet thicknesses and roller power required but also in calculating the relationships among roller deflections, roller speed, and fluctuations in reservoir feed within a control loop designed for maintaining uniform exit height. A digital simulation of a calendering system could be written to show the feasibility of such a control loop and would be a valuable design tool.

Two natural extensions of this work are the prediction of roller pressure distribution as described in the preceding section and treating the two-dimensional case. In this case, the flow occurs parallel to the roller axes as well as through the rollers. This can be done by dividing the nonuniform reservoir into sectors of uniform width as illustrated in Figure 12. Then, by incrementing time, spread patterns of thickness versus the x- and y-coordinates could be predicted.

In the future, rheological problems involving more sophisticated models such as those of Oldroyd,[8] Carreau,[9] and others might be solved numerically. It is hoped that this work represents a significant step in that direction.

Nomenclature

A	fluid constant, see eq. (3)
B	fluid constant, see eq. (3)
h	roller separation
h_1	fluid thickness at exit
H	roller separation (gap) at reservoir
H_0	minimum roller separation
k	fluid constant, see eq. (3)
N	number of data points to be fit by curve
n	fluid constant, see eq. (3)
P	pressure
Q	flow rate
R	roller radius
t	time
U	roller surface speed
x	distance from roller nip along axis of symmetry
x_1	x at fluid exit
x_{RES}	x at tip of reservoir
y	distance from axis of symmetry

$\dot{\gamma}$ shear rate
η apparent viscosity
μ Newtonian viscosity
ρ density
τ shear
τ_w shear at roller surface
ϕ $x/\sqrt{2RH_0} = \sqrt{(h/H_0) - 1}$
ϕ_1 $x_1/\sqrt{2RH_0} = \sqrt{(h_1/H_0) - 1}$
ϕ_H $x_{RES}/\sqrt{2RH_0} = \sqrt{(H/H_0) - 1}$

References

1. J. M. McKelvey, 1962, *Polymer Processing*, Wiley, New York, 1962.
2. R. E. Gaskell, *J. Appl. Mech.*, **17**, 344 (1950).
3. J. S. Chong, *J. Appl. Polym. Sci.*, **12**, 191 (1968).
4. C. R. Wylie, Jr., *Advanced Engineering Mathematics*, McGraw-Hill, New York, 1966.
5. I. Brazinsky, H. Cosway, R. C. Jones, V. Story, and C. F. Valle, *J. Appl. Polym. Sci.*, **14**, 2781 (1970).
6. B. W. Arden and K. N. Astill, *Numerical Algorithms, Origins and Applications*, Addison-Wesley, Reading, Mass., 1970.
7. W. W. Alston, Jr., B. S. Thesis, Dept. of Mechanical Engineering, Tufts University, Medford, Mass., 1971.
8. J. G. Oldroyd, in *Rheology*. Vol. I, Academic Press, New York, 1956, Chap. 16.
9. J. P. Carreau, 1968, Ph.D. Thesis, University of Wisconsin, 1968, in preparation for publication.

Additional References

R. B. Bird, W. E. Stewart, and E. N. Lightfoot, *Transport Phenomena*, Wiley, New York, 1960.
J. S. Chong and D. M. Vezzi, *J. Appl. Polym. Sci.*, **14**, 17 (1970).
S. D. Conte, *Elementary Numerical Analysis*, McGraw-Hill, New York, 1965
S. S. Kuo, *Numerical Methods & Computers*, Addison-Wesley, Reading, Mass., 1965.
Marshall, D. I., in *Processing of Thermoplastic Materials*, Reinhold, New York, Chap. 6.

Received July 5, 1972
Revised March 28, 1973